JOURNAL OF GEOPHYSICAL RESEARCH, VOL. 86, NO. C12, PAGES 12,071–12,081, DECEMBER 20, 1981

Observations of Ozone Depletion Associated With Solar Proton Events

R. D. McPeters, C. H. Jackman, and E. G. Stassinopoulos

Laboratory for Planetary Atmospheres, NASA, Goddard Space Flight Center, Greenbelt, Maryland 20771

Data from the backscattered ultraviolet instrument (BUV) on Nimbus 4 show depletion of ozone following solar proton events in January and September 1971 and in August 1972. The direct effect of high energy protons on the BUV instrument was determined by comparing nighttime BUV counting rates with particle data from IMP 6. The instrumental effects were then subtracted to allow accurate calculation of ozone profiles during the three events. The solar proton event of August 1972 was very large and produced an ozone depletion of 15% at 42 km that persisted for almost 30 days. This long recovery time indicates that NO_x was produced in a quantity sufficient to alter the ozone chemistry. The two proton events in 1971 were of moderate size but produced ozone depletions of 10–30% at 50 km with a 36-hour recovery time. The rapid recovery is consistent with the assumption that HO_x was responsible for altering the ozone chemistry, but the magnitude of the observed depletion exceeds that predicted by our chemical models.

1. Introduction

The chemistry of the upper stratosphere is imperfectly understood because of the large number of possible reactions and uncertainties in the concentrations and reaction rates of the various species. We can gain valuable insight into the chemistry by observing the response of ozone to changes in individual species. Gradual changes, such as those caused by the introduction of chlorofluoromethanes, are difficult to distinguish from the normal background variability and require accurate long-term monitoring programs for accuracy. But during a solar proton event NO_x (N, NO, and NO_2) and HO_x(H, OH, and HO_2) are produced very rapidly (during the hours of the event itself) and in a limited area of the globe (above about 60° geomagnetic latitudes), and this signature makes the resulting changes in ozone relatively easy to identify. SPEs (solar proton events) therefore act as natural 'experiments' that can be used to check elements of the stratospheric chemistry problem.

The first measurement of changes in ozone resulting from SPEs was reported by *Weeks et al.* [1972]. Rockets fired during and after the November 2, 1969, SPE showed a large decrease in ozone even at 52 km, the lowest altitude observed. The atmospheric chemistry required to explain such a depletion was developed by *Swider and Keneshea* [1973] and further revised by *Frederick* [1976] and *Swider et al.* [1978]. *Heath et al.* [1977] reported an observation by the backscattered ultraviolet instrument (BUV) on the Nimbus 4 satellite of an ozone decrease following the very large SPEs of August 1972. *Crutzen et al.* [1975] had earlier predicted that NO produced by SPEs could catalytically destroy significant amounts of ozone. Recently, *Borucki et al.* [1978], *Fabian et al.* [1979], *Reagan et al.* [1981], *Solomon and Crutzen* [1981], and *Rusch et al.* [1981] have worked on modeling various aspects of the August 1972 SPEs.

In this paper we reanalyze the August 1972 SPEs, using the reprocessed BUV data set, and report our analysis of two smaller SPEs in January and September 1971. The ozone data from Nimbus 4 BUV have been reprocessed and are now available from the National Space Science Data Center at the Goddard Space Flight Center. Instrument errors were corrected; the calibration was much better maintained; and the inversion algorithm now uses a better first guess, more wavelengths, and a multiple scattering correction. The results for the August 1972 SPEs confirm the ozone decrease reported by *Heath et al.* [1977], differing only in detail. The SPEs in 1971 were similar in magnitude to the 1969 SPE observed by *Weeks et al.* [1972] and, our analysis shows, produce ozone depletion near the stratopause of similar magnitude. In the next three sections we present details of our analysis of the satellite data showing ozone depletion associated with SPEs, and in the final sections we give a theoretical analysis of the atmospheric chemistry during these SPEs.

2. Instrument Effects and Radiance Correction

During an SPE, protons penetrate the satellite and photomultiplier tubes to produce a wavelength independent background signal analogous to a dark current signal. If uncorrected, this direct instrumental effect of protons can cause serious errors in the radiances measured at the profiling wavelengths (below 300 nm). To establish the existence of ozone depletion during an SPE we must accurately correct our radiances for contamination.

Fortunately, we have a way to predict the effect of particles on the instrument. In 1970 and 1971 the instrument was operated in the pulse counting mode for the night half of each orbit, so we have direct measurements of the effect of protons on the instrument during the 1971 SPEs. Before an event, the pulse counter at night shows from 2000 counts per second (cps) in most regions to 10,000 cps in the electron horn region near 60° geomagnetic latitude. For comparison, the radiance at 273.5 nm near 80° solar zenith angle is equivalent to 550,000 cps. During an SPE, we observe normal counting rates up to 55° geomagnetic latitude, a steep gradient, then a relatively constant counting rate above 60° geomagnetic latitude over the polar cap to the terminator. The variance of the counting rate over the polar cap is about 10% at high flux levels (>100,000 cps) increasing to 20% at low flux levels (<20,000 cps). No trend of counting rate with position over the polar cap is clear in either the January or September SPE.

To obtain a better interpolation of counting rate versus

Paper number 1C1409.

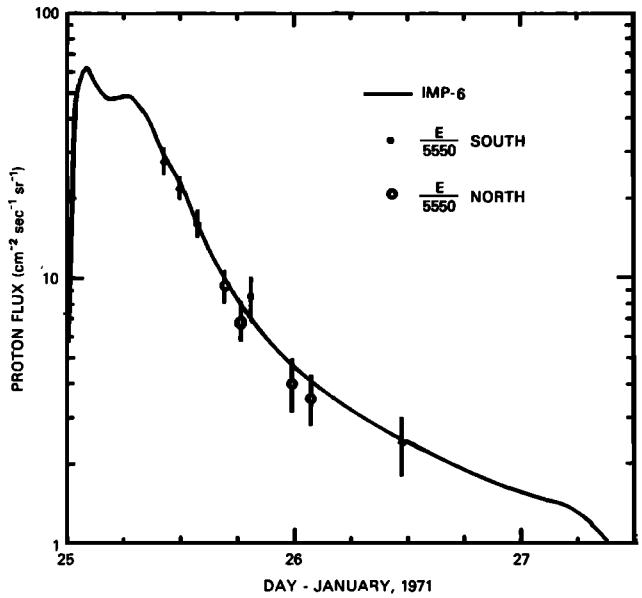

Fig. 1. A comparison of the proton flux measured by IMP-6 (extrapolated to $E > 72$ MeV) with nighttime counting rates (E) measured by BUV above 58° geomagnetic latitude in northern and southern hemispheres.

time during the 1971 SPEs and to predict the instrument contamination during the August 1972 SPEs when BUV no longer operated at night, we compared the BUV derived counting rates with the proton flux measured by IMP 6 (Explorer 43). IMP measures integral fluxes of protons for energies >60, >30, and >10 MeV. In seeking a direct relationship between IMP proton fluxes and BUV counting rates we are assuming first, that the solar proton flux outside the earth's magnetic field is directly related to that at Nimbus orbital altitude (1100 km) at latitudes above 60° geomagnetic and, second, that the BUV photomultiplier in this domain responds to protons only of energy greater than some limit.

In Figures 1 and 2 we show that a simple multiplicative constant can be found to relate IMP and BUV. If we assume that only protons of energy >72 MeV penetrate the BUV satellite to the photomultiplier tube, we find that a single multiplicative factor, 5550 (counts s^{-1})/(protons cm^{-2} s^{-1} sr^{-1}), relates IMP fluxes to BUV nighttime counting rates for both the January and the September 1971 SPEs. The energy spectra of the two events were quite different. At 10 and 30 MeV, the January SPE was much larger than the September SPE, but at 60 MeV the two events were almost equal. The result is that if we assume a BUV cutoff energy other than about 72 MeV, we find substantially different multiplicative factors for the two events. Moreover, because high energy protons arrive sooner than low energy protons, we must assume 72 MeV protons to match the time history of the September SPE as measured by BUV (Figure 2). Thus, we have two compelling reasons for assuming a 72 MeV cutoff. In extrapolating the IMP measurements at 30 MeV and 60 MeV to 72 MeV, we assume an exponential energy dependence. Energy spectra published by *Reagan et al.* [1981] show that this is not exactly true but indicate that the error in extrapolating only 12 MeV should be small.

During the January SPE we happen to have BUV nighttime counting rates in both northern and southern hemispheres (Figure 1). The northern hemisphere rates appear to be about 15% higher than the southern. The axial tilt of the earth in January could be expected to favor slightly the acceptance of particles into the northern polar region.

The accuracy with which we can correct the measured radiances for particle contamination depends on the accuracy to which the contamination is known and the size of the signal due to particles relative to the size of the signal due to backscattered sunlight. In the January and September 1971 SPEs, the peak contribution due to particles equals the signal from backscattered sunlight; and at the peak of the first August 1972 SPE the contamination is 30 times the expected radiance. Given the 10–20% uncertainty in the proton count rate, we should not attempt to correct radiances so heavily contaminated. Instead, we have set an upper limit of 200,000 cps for radiance correction. While the proton contamination is independent of wavelength, the backscattered radiance increases rapidly between 273.5 and 305.8 nm (the shortest and longest wavelengths used for ozone profile retrievals) because of the decreasing ozone absorption coefficient. For large solar zenith angles a proton contamination level of 200,000 cps represents 50% of the backscattered radiance at 273.5 nm, 20% of the radiance at 287.6 nm, and only 10% of the radiance at 297.5 nm. If there is a 20% uncertainty in our estimate of proton contamination, the uncertainty in our corrected radiances at the same wavelengths will be only 10, 4.4, and 2%, respectively. These estimates should represent upper limits on the radiance uncertainty; at lesser proton flux levels or smaller zenith angles the percent radiance uncertainty should be proportionately less.

3. Observed Ozone Depletion in 1971 SPEs

In Figures 3 and 4 we show the ozone depletion deduced from the BUV measurements for the moderate SPEs of January 25, 1971, and September 2, 1971. The radiances for each scan were corrected for an instantaneous proton flux level derived from Figures 1 and 2. Here the IMP 6 proton

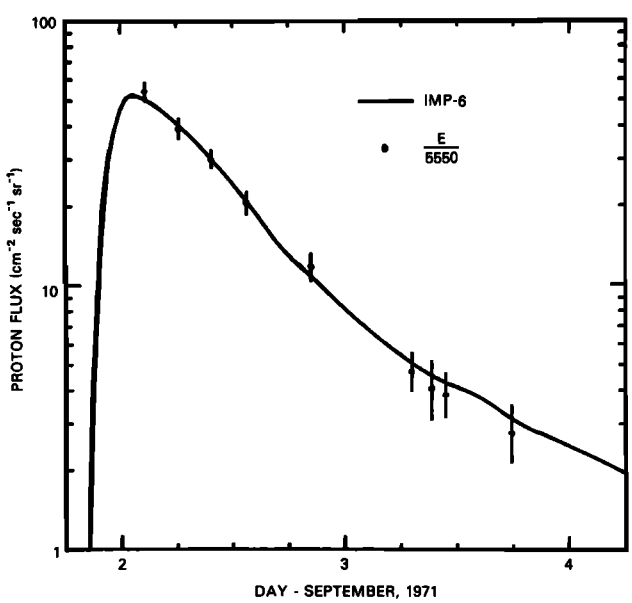

Fig. 2. A comparison of the proton flux measured by IMP-6 ($E >$ 72 MeV) in September 1971 with nighttime counting rates measured by BUV above 58° geomagnetic latitude in the southern hemisphere.

measurements are being used primarily for interpolation; the absolute level is controlled by the BUV nighttime measurements. The corrected radiances were then used to invert ozone profiles, which are shown in Figures 3 and 4 for three levels in the atmosphere: 0.5, 1, and 2 mbar, corresponding approximately to 56, 50, and 44 km, respectively. Points are plotted for each orbit of available data. Tests of the profile inversion algorithm indicate that accurate ozone profiles should be retrieved even during an SPE. A radical departure from the shape of the a priori profile could cause problems (for instance, if ozone were severely depleted in a 5-km layer only to produce a double peaked profile). But the profile shape changes predicted by theoretical computation should not cause problems.

One problem in determining an ozone depletion is the normal ozone gradient with geodetic latitude that exists in the polar region. If we plot the data for constant geomagnetic latitude, large variations are seen depending on the geodetic latitude for a particular scan. We choose to plot data for constant geodetic latitude to minimize the gradient problems. This is reasonable if the proton flux is uniform above 60° geomagnetic latitude, as our nighttime data indicate, and if we do not use data below about 70° geodetic latitude.

In Figure 3 we plot data at 75°S geodetic latitude for the January SPE for each orbit. The level of normal ozone and its uncertainty and variability are indicated by the preevent data. It is clear that an ozone depletion of much less than 10% would be difficult to distinguish because of the variability and sparseness of the data. Ignoring the initial point of day 25 for reasons that will be explained later, we see an ozone depletion of 20–30% at 1 mbar on day 25 decreasing to near zero by the end of the day. Even larger depletion is seen at 0.5 mbar, but the results there are more susceptible to error.

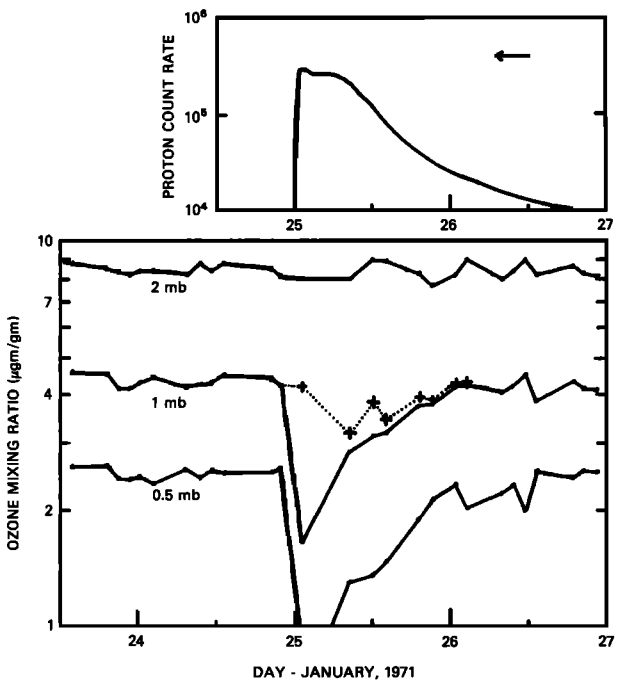

Fig. 3. The ozone mass mixing ratio at three levels retrieved by using corrected radiances during the January 1971 SPE plotted below the IMP interpolated proton counting rate. The dotted curve represents a lower limit ozone depletion. The arrow marks the equivalent counting rate of the 273.5 nm radiance. Data at 75°S latitude.

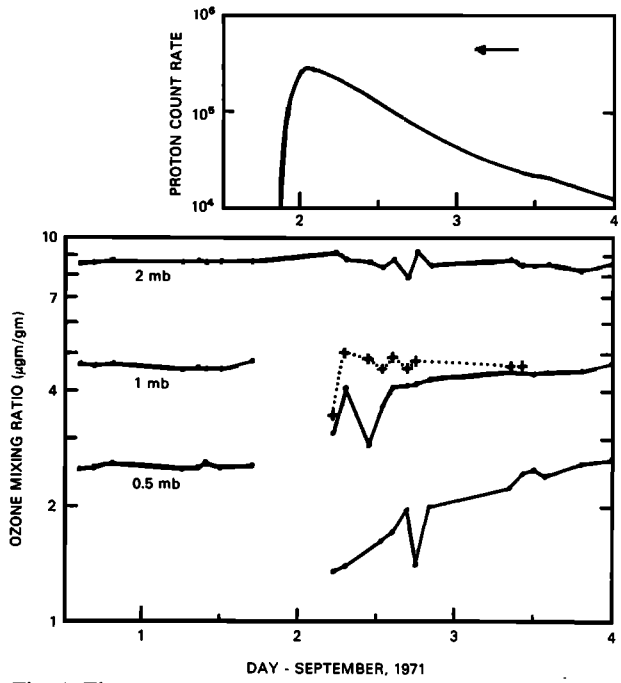

Fig. 4. The ozone mass mixing ratio at three levels retrieved by using corrected radiances during the September 1971 SPE plotted below the IMP interpolated proton counting rate. Data from geodetic latitude band at 75°N to 80°N.

At 2 mbar any ozone depletion is indistinguishable from preevent variability. The results shown in Figure 4 for the September SPE follow much the same pattern.

The most serious obstacle to interpreting these observations as real ozone depletion is the very high level of 'noise' in the radiances (and derived ozone) during the SPE. Before the January SPE, ozone at 1 mbar at 75°S latitude has a 4% variability because of random digitization errors and variability of ozone with latitude and longitude. But during the SPE on day 25 hour 8 the 1 mbar ozone derived by using corrected radiances exhibits scan to scan variations along the orbital track of 20%. This variability decreases to about 10% by the hour 12 orbit and to about 5% by hour 14. The nighttime measurements indicate a variability in the proton flux of about 10%, and this should translate into only a few percent variability in ozone even at hour 8. Part of the explanation is that the daylight readings, instead of being a 1.8 s integrated readings, are an average of four short interval readings at each wavelength. The result is that the daytime readings have a higher statistical variability in the proton component of the signal than indicated by the nighttime data. Also we cannot rule out the possibility that the proton flux itself is more variable on the dayside than on the nightside; we have explicitly assumed the day/night proton flux to be about the same.

In view of the high variability and some uncertainty about our assumptions, can we be sure that we are seeing a real effect? If our estimates of the dayside proton count rate were in error by a factor of 2, the depletion we see could be explained as purely contamination. To disprove this possibility, we have made an upper limit proton flux calculation. The 255.5-nm channel, which is not used for profiling for other reasons, is most sensitive to proton contamination. We force the 255.5-nm radiance to equal its average preevent value

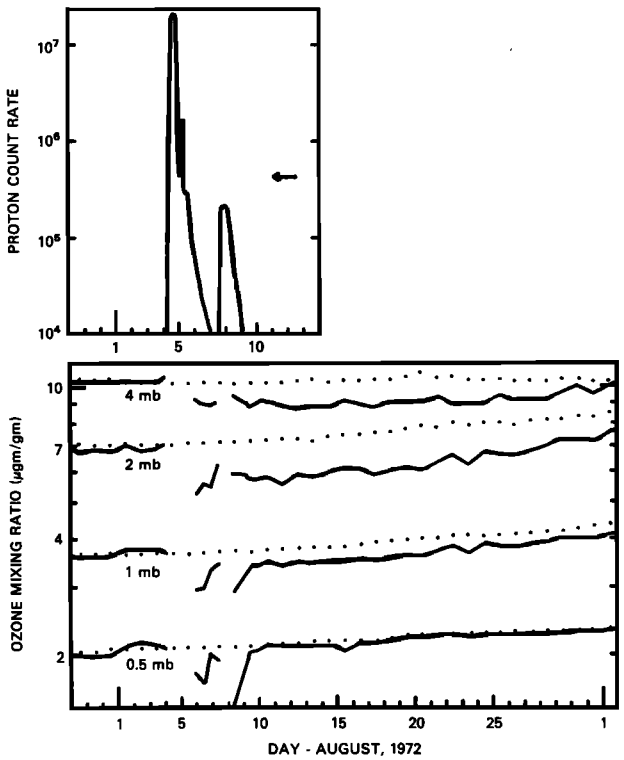

Fig. 5. The ozone mass mixing ratio at four levels during August 1972 plotted below the IMP derived counting rates. The data are 1-day zonal averages for a latitude band at 69°N to 77°N for geomagnetic latitudes greater than 62°. The dotted curve represents the 'normal' ozone mixing ratio of August 1970.

and attribute all the excess signal to protons. In doing this we are assuming that there is zero ozone depletion at the altitude of the 255.5-nm contribution function (about 56 km). If there actually is no ozone depletion, the proton counting rate so derived will be correct, and the true ozone profile will be inverted at all altitudes. If an ozone depletion does exist, we will erroneously attribute radiance change due to ozone depletion near 0.5 mbar to increased proton flux. A depletion will still be calculated in the 45- to 50-km region but underestimated by from 10 to 60%, depending on the ozone altitude dependence. This is possible because the proton contribution is a decreasing fraction of the total radiance at the longer wavelengths that penetrate further into the atmosphere and consequently have more backscattered radiation.

This upper limit procedure for estimating the proton flux was used to calculate the dotted curves at 1 mbar in Figures 3 and 4. In Figure 3 the first point on day 25 now shows zero depletion; we probably slightly missed the exact starting time of the SPE because the IMP-6 data are 1 hour averages, and there really was no ozone depletion at this time. But the remaining points on that day show about the same level of depletion, whether calculated by using IMP derived proton fluxes or by using the upper limit 255.5 nm proton flux. This is strong evidence that there was a real ozone depletion at 50 km during the SPE of January 25, 1971.

The results for the September SPE, on the other hand, are ambiguous. In Figure 4 the point at hour 6 on day 2 still shows a strong depletion, but the remaining points show no depletion. This is a lower limit depletion calculation, and such a result would be found if the ozone depletion increased rapidly between 50 and 55 km (1–0.5 mbar). But based on the results here, we cannot conclude with certainty that there was ozone depletion during the September 1, 1971, SPE.

4. Observed Ozone Depletion in August 1972

In Figures 5 and 6 we show details of the recalculated ozone depletion and recovery that followed the very large SPEs of August 4 and August 7, 1972, the depletion first reported by *Heath et al.* [1977]. In Figure 5 we plot the ozone mixing ratio as a function of time for four altitudes. Each point is a 1-day zonal average of about 12 individual scans. We see a sharp decrease in ozone during the SPEs that disappears as the proton flux returns to normal, much the same behavior as seen in the 1971 SPEs. But here a long-term depletion of ozone is seen that persists for almost a month after the SPEs have ended. The proton counting rates used to correct radiances during the 1972 SPEs are derived solely from IMP 6 measurements analyzed in the same way as IMP data for the 1971 SPEs.

To estimate the long-term ozone depletion accurately, we must take into account normal seasonal behavior. In Figure 5 the dotted curves show the normal seasonal trends determined for the same time period in 1970, when data coverage was highest. There was very clearly an ozone depletion following the August 1972 SPEs that persisted for at least a month. A similar depletion is observed by BUV in the southern hemisphere, but the data are much more difficult to analyze. BUV does not retrieve profiles for solar zenith angles greater than 86°, and in the southern hemisphere in August this restricts us to latitudes less than 67°. Thus, only a limited amount of data is available. Moreover, ozone in the upper stratosphere is highly variable in the winter and exhibits a steep gradient with latitude [*McPeters*, 1980]. But when we compare a 1-week average of preevent data with a 1-week average of data immediately after the SPE, we find a 13% decrease at 2 mbar in the southern hemisphere. The

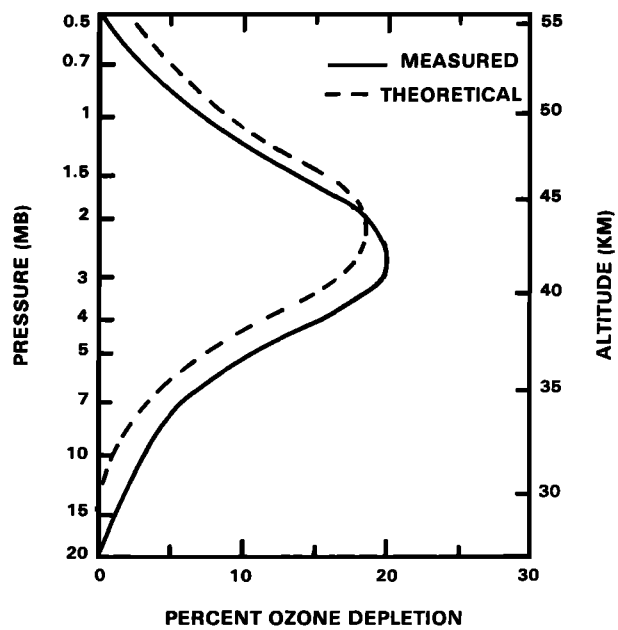

Fig. 6. The percentage ozone decrease versus pressure (altitude) 2 weeks after the August 1972 SPEs, corrected for seasonal variation. For comparison recent theoretical results of *Rusch et al.* [1981] are shown.

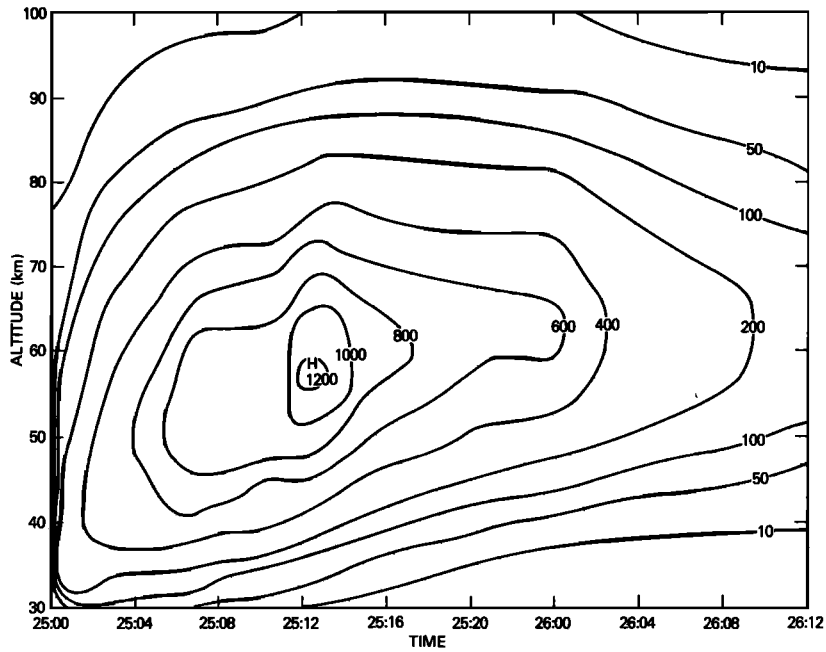

Fig. 7. Ion pair production contours in (cm^{-3} s^{-1}) for the January 1971 SPE. Time is given in day:hour (GMT).

mass mixing ratio at 2 mbar before the SPE was 10.31 ± 0.64, while after the SPE it was 9.06 ± 0.62, where we have given the 2σ standard error. This is further evidence confirming the observed ozone depletion to be caused by solar protons.

5. Theoretical Discussion

Solar protons produce both NO_x and HO_x species. These NO_x and HO_x species have different lifetimes, but both induce ozone depletion through catalytic cycles. In the upper stratosphere the NO_x lifetimes tend to be long (~ months) while the HO_x lifetimes tend to be short (less than an hour). The two species, therefore, have characteristic ozone depletion signatures that might be seen in the observational data.

The relatively sharp decreases in ozone observed during the initial hours of the August 1972 SPEs, illustrated in Figure 5, are mainly attributed to the HO_x species, while the long-term depletion is probably caused by the NO_x. The 1971 SPEs indicate ozone depletions only during the events and thus are probably due to the HO_x species.

The ozone depletion induced by solar proton produced NO_x has been discussed extensively in the literature [*Crutzen et al.*, 1975; *Frederick*, 1976; *Reid et al.*, 1976; *Borucki et al.*, 1978; *Heaps*, 1978; *Fabian et al.*, 1979; *Reagan et al.*, 1981; *Solomon and Crutzen*, 1981; *Rusch et al.*, 1981]. In Figure 6 theoretical results are compared with the measured percentage ozone decrease as a function of altitude averaged over the period August 14–19 and adjusted for the normal seasonal variation. The HO_x effects should have died away by this time but transport effects should still be negligible. The theortical calculations plotted in Figure 6 were made by *Rusch et al.* [1981] for the August 1972 SPEs. These theoretical calculations for 8 days from the beginning of the SPEs are taken from Figure 7 (model A) of the Rusch et al. paper. The theortical curve agrees well with the experimental curve, only shifted verticaly by about 1 km. In general, therefore, the initial ozone depletion due to the NO_x seems to be fairly well understood. The subsequent mixing and transport of the enhanced NO_x and depleted O_3 air mass from the polar latitudes into the middle latitudes deserves further study with more sophisticated models [*Reagan et al.*, 1981].

We do not consider this NO_x transport problem but instead focus our theoretical work on the more immediate problem of explaining the HO_x induced ozone depletion signature of the 1971 SPEs. Several papers are in the literature concerning ozone depletion resulting from the HO_x species produced during SPEs [*Swider and Keneshea*, 1973; *Frederick*, 1976; *Swider et al.*, 1978; *Heaps*, 1978; *Crutzen and Solomon*, 1980; *Solomon et al.*, 1981]. These papers concentrate on the HO_x-induced ozone depletions in the mesosphere. Our data for the January 1971 SPE (Figure 3) show a substantial depletion of ozone at the 1-mbar level (approximately 50 km). Large decreases in ozone near 70 km are relatively easy to justify from moderate SPEs, but large decreases at 50 km are very difficult to justify.

6. Photochemical Equilibrium Model Results

Since the atmosphere is fairly close to steady state at 50 km we have constructed a simple photochemical equilibrium model for that altitude by using the equations given in the appendix and the reactions and their rates given in Table 1. At 50 km altitude there is an equilibrium between destruction of O_3 through photolysis

$$O_3 + h\nu \rightarrow O_2 + O$$

or

$$O_3 + h\nu \rightarrow O_2(^1\Delta) + O(^1D)$$

and production of O_3 through recombination

$$O_2 + O + M \rightarrow O_3 + M$$

Because of the significance of O in the formation of O_3, loss of O is the same as loss of O_3.

The most important HO_x catalytic cycle for O_x (O and O_3) destruction is the following:

TABLE 1. Reactions and Their Rates Used in the Photochemical Equilibrium Model

Reaction	Rate
$O_2 + h\nu \rightarrow O + O$	$J_1 = 5.98 \times 10^{-10}$*
$O_3 + h\nu \rightarrow O_2 + O$	$J_2 = 4.07 \times 10^{-4}$
$O_3 + h\nu \rightarrow O_2 (^1\Delta) + O(^1D)$	$J_3 = 3.51 \times 10^{-3}$
$H_2O + h\nu \rightarrow H + OH$	$J_4 = 3.96 \times 10^{-9}$
$NO_2 + h\nu \rightarrow NO + O$	$J_5 = 1.05 \times 10^{-2}$
$HO_2 + h\nu \rightarrow OH + O$	$J_6 = 3.94 \times 10^{-4}$
$HCl + h\nu \rightarrow H + Cl$	$J_7 = 2.06 \times 10^{-7}$
$HOCl + h\nu \rightarrow OH + Cl$	$J_8 = 2.80 \times 10^{-4}$
$O + O_2 + M \rightarrow O_3 + M$	$k_1 = 6.2 \times 10^{-34} (T\dagger/300)^{-2}$
$O + O_3 \rightarrow O_2 + O_2$	$k_2 = 1.5 \times 10^{-11} \exp(-2218/T)$
$OH + O \rightarrow O_2 + H$	$k_3 = 4.0 \times 10^{-11}$
$OH + O_3 \rightarrow O_2 + HO_2$	$k_4 = 1.6 \times 10^{-12} \exp(-940/T)$
$HO_2 + O \rightarrow O_2 + OH$	$k_5 = 3.5 \times 10^{-11}$
$HO_2 + O_3 \rightarrow O_2 + O_2 + OH$	$k_6 = 1.1 \times 10^{-14} \exp(-580/T)$
$OH + HO_2 \rightarrow O_2 + H_2O$	$k_7 = 4.0 \times 10^{-11}$
$NO_2 + O \rightarrow O_2 + NO$	$k_8 = 9.3 \times 10^{-12}$
$NO + O_3 \rightarrow O_2 + NO_2$	$k_9 = 2.3 \times 10^{-12} \exp(-1450/T)$
$O(^1D) + H_2O \rightarrow OH + OH$	$k_{10} = 2.3 \times 10^{-10}$
$O(^1D) + N_2 \rightarrow O + N_2$	$k_{11} = 2.0 \times 10^{-11} \exp(107/T)$
$O(^1D) + O_2 \rightarrow O + O_2$	$k_{12} = 2.9 \times 10^{-11} \exp(67/T)$
$Cl + O_3 \rightarrow ClO + O_2$	$k_{13} = 2.8 \times 10^{-11} \exp(-257/T)$
$ClO + O \rightarrow Cl + O_2$	$k_{14} = 7.7 \times 10^{-11} \exp(-130/T)$
$OH + HCl \rightarrow H_2O + Cl$	$k_{15} = 2.8 \times 10^{-12} \exp(-425/T)$
$Cl + HO_2 \rightarrow HCl + O_2$	$k_{16} = 4.5 \times 10^{-11}$
$HO_2 + ClO \rightarrow HOCl + O_2$	$k_{17} = 5.2 \times 10^{-12}$
$Cl + CH_4 \rightarrow HCl + CH_3$	$k_{18} = 9.9 \times 10^{-12} \exp(-1359/T)$

All rates except photodissociation rates come from *Hudson and Reed* [1979].

*The values reported for the photodissociation rates refer to a sun angle of 75° and at an altitude of 50 km. The units are in s^{-1}.

†Temperature T is in degrees Kelvin. Rate coefficients for two-body reactions are in $cm^3\ s^{-1}$; the values for the three-body reactions are in $cm^6\ s^{-1}$.

$$\begin{aligned} &O + OH \rightarrow H + O_2 \\ &H + O_2 + M \rightarrow HO_2 + M \\ &O + HO_2 \rightarrow OH + O_2 \\ \hline &\text{net: } O + O \rightarrow O_2 \end{aligned}$$

Other major loss schemes for O_x are due to the Chapman mechanism and catalytic cycles with NO_x and Cl_x species. By using a temperature of 277°K (60° latitude summer, Cira (1972)) and fixing several species (H_2O, NO, CH_4, HCl, HOCl, M, N_2, and O_2), the species O_3, $O(^3P)$, $O(^1D)$, OH, HO_2, NO_2, ClO, and Cl were all solved self-consistently and are given in column A of Table 2. In this case the individual loss terms for O_x (from (A3) of the appendix) and their values in $(cm^{-3}\ s^{-1})$ are

$$2k_2\,[O]\,[O_3] = 3.31 \times 10^6$$

$$2k_3\,[OH]\,[O] = 5.60 \times 10^6$$

$$2k_8\,[NO_2]\,[O] = 6.15 \times 10^5$$

$$2k_{14}\,[ClO]\,[O] = 4.90 \times 10^5$$

The largest loss term for the O_x species is that due to the HO_x species, while the second largest is that due to the Chapman mechanism. The NO_x and Cl_x (Cl and ClO) species account for only about 11% of the O_x loss term.

The HO_x species are self-regulating with the reaction

$$OH + HO_2 \rightarrow H_2O + O_2$$

being the major means of destruction at 50 km. Any increase in HO_x speeds up this reaction and shortens the HO_x species' lifetimes.

The HO_x species are produced in two major ways, either by the reaction

$$H_2O + O(^1D) \rightarrow 2OH$$

or through photolysis

$$H_2O + h\nu \rightarrow H + OH$$

In the case of photochemical equilibrium at 50 km, the HO_x production in units of $(cm^{-3}\ s^{-1})$ for these two paths are

$$2k_{10}[H_2O]\,[O(^1D)] = 2.58 \times 10^4$$

and

$$2J_4[H_2O] = 2.75 \times 10^3$$

During an SPE HO_x is produced when solar protons produce positive ions which in turn produce ion water clusters along with H and OH. Most of the positive ions result in the formation of two HO_x species apiece at least up to 70 km [*Frederick*, 1976; *Crutzen and Solomon*, 1980]. Above 75 km the HO_x species produced per positive ion depend quite strongly on the ionization rate and the duration

TABLE 2. Species' Number Densities for the Null SPE Case

Species	A	B	C	D	E
O_3	8.18 + 10*	8.40 + 10	7.74 + 10	7.62 + 10	6.51 + 10
$O(^3P)$	4.06 + 9	4.17 + 9	3.84 + 9	4.03 + 9	3.70 + 9
$O(^1D)$	4.03 + 2	4.14 + 2	3.81 + 2	3.75 + 2	3.51 + 2
OH	1.73 + 7	1.77 + 7	1.30 + 7	1.94 + 7	1.49 + 7
HO_2	2.02 + 7	2.07 + 7	1.50 + 7	1.80 + 7	1.40 + 7
NO_2	8.15 + 6	8.19 + 6	8.06 + 6	9.38 + 6	8.04 + 6
ClO	1.25 + 6	···	···	···	···
Cl	2.70 + 5	···	···	···	···
H_2O	1.39 + 11	1.39 + 11	3.80 + 10	1.39 + 11	3.80 + 10
NO	3.80 + 8	3.80 + 8	3.80 + 8	3.97 + 8	3.77 + 8
CH_4	7.59 + 9	···	···	5.94 + 9	5.13 + 9
HCl	3.80 + 7	···	···	···	···
HOCl	5.06 + 5	···	···	···	···
M	2.53 + 16	2.53 + 16	2.53 + 16	2.53 + 16	2.53 + 16
N_2	2.00 + 16	2.00 + 16	2.00 + 16	2.00 + 16	2.00 + 16
O_2	5.33 + 15	5.33 + 15	5.33 + 15	5.33 + 15	5.33 + 15

In cm^{-3}. Columns A–C show those used in the photochemical equilibrium model, and columns D and E show those used in the one-dimensional time-dependent model at 50 km altitude.

*8.18 + 10 means 8.18×10^{10}

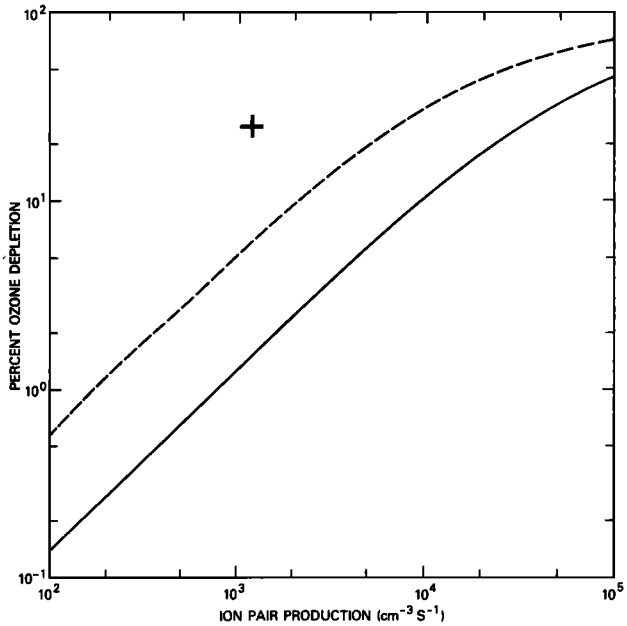

Fig. 8. The percentage ozone decrease as a function of the ion pair production at 1 mbar (50 km). The plus sign represents the ozone decrease observed at the maximum ionization rate of the January 1971 SPE. The solid line presents the results, using regular chemistry and reasonable H_2O concentration, in the photochemical equilibrium model. The dashed line presents the results, using modified chemistry and low H_2O concentration, in the photochemical equilibrium model.

of the SPE [*Solomon et al.*, 1981]. Since we are mainly concerned with the upper stratospheric and lower mesospheric region in this paper, we assume that $S_{HO_x} = 2\ I_p$, where I_p is the ionization rate and S_{HO_x} is the HO_x production rate. Therefore, at 50 km the I_p must have a value of a few thousand ion pairs $cm^{-3}\ s^{-1}$ or the S_{HO_x} must have a value of several thousand ion pairs $cm^{-3}\ s^{-1}$ for there to be a substantial change in the HO_x and O_3 concentrations due to an SPE.

Using the particle energy deposition approach discussed in *Jackman et al.* [1980] with the IMP 6 particle fluxes from *Natural Oceanic and Atmospheric Administration* [1971], we calculated the hourly ion pair production due to the January 1971 SPE. This ion pair production is given in Figure 7 for the January 1971 SPE. The maximum ionization rate for this event is $9.5 \times 10^2\ cm^{-3}\ s^{-1}$ at 50 km and $1.2 \times 10^3\ cm^{-3}\ s^{-1}$ at 55 km. Even if we assume that the ionization rate of $1.2 \times 10^3\ cm^{-3}\ s^{-1}$ really occurs at 50 km, this still only results in an S_{HO_x} value of $2.4 \times 10^3\ cm^{-3}\ s^{-1}$, which is small in comparison with the ambient HO_x production rate of $2.86 \times 10^4\ cm^{-3}\ s^{-1}$. An ozone decrease of 1.5% at 50 km results from the use of this S_{HO_x} value in the photochemical equilibrium model in contrast with the approximately 25% ozone decrease observed.

We calculated the ozone decrease resulting from a number of different values of I_p and present those calculations with the solid curve in Figure 8. Decreases in ozone of the magnitude observed during the January 1971 SPE would require values of I_p greater than $7 \times 10^3\ cm^{-3}\ s^{-1}$.

Since values of I_p of this magnitude are unrealistic for the January 1971 SPE, we focused our attention on the photochemical equilibrium model and its input. (Recent recommended changes in reaction rates [*DeMore et al.*, 1981] do not result in substantial changes in the photochemical equilibrium model results.)

Omission of the chlorine chemistry gave ozone decreases less than 2% higher than those observed with the inclusion of the chlorine chemistry (at an $I_p = 1.2 \times 10^3\ cm^{-3}\ s^{-1}$ the ozone decrease equals 1.53% including chlorine chemistry and equals 1.50% without including chlorine chemistry). The species' densities for this case are presented in column B of Table 2. A plot of the percentage of ozone decrease as a function of the I_p without including chlorine chemistry would be virtually indistinguishable from the solid line of Figure 8, and thus it is not plotted. Since this change is not substantial and the omission of the chlorine simplified the chemistry a great deal, all subsequent calculations are completed without the use of any chlorine species.

Because of the large discrepancy between the theory and atmospheric observations, we completed a sensitivity study to detemine which parameters were most influential in determining the eventual ozone decrease due to the HO_x species. The reaction rates k_3, k_5, k_7, the H_2O concentration, and the solar zenith angle all have a large influence on the eventual decrease in ozone resulting from the SPEs. An increase in k_3 results in an increase in the loss of O_x due to the HO_x species (see (A3)). An increase in k_5 results in an increase in OH with respect to HO_2 (see (A8)) and, therefore, in an increase in the HO_x term in (A3). A decrease in k_7 results in a reduction of HO_x specie loss. The effect of this is an increase in the HO_x species since (A16) is rewritten without chlorine chemistry as

$$[OH] = \left[\frac{2k_{10}\,[H_2O]\,[O(^1D)] + 2J_4\,[H_2O] + S_{HO_x}}{2k_7 R}\right]^{1/2}$$

A decrease in the H_2O concentration reduces the subsequent ambient HO_x production given by $2k_{10}\,[H_2O]\,[O(^1D)]$ and $2J_4\,[H_2O]$ and thus increases the influence of the SPE. An increase in the solar zenith angle has the same effect as a decrease in the H_2O concentration. Increasing the solar zenith angle leads to a decrease in the $O(^1D)$ concentration and to a decrease in the J_4 and, consequently, increases the influence of the SPE. Since the Nimbus 4 satellite observed at a relatively constant solar zenith angle in the polar regions, its value was not changed in the following calculation.

We adjusted k_3, k_5, k_7, and the H_2O concentration to their limits of believability in an attempt to reproduce the observed ozone depletion. The reaction rate k_3 was changed from $4.0 \times 10^{-11}\ cm^3\ s^{-1}$ to $6.5 \times 10^{-11}\ cm^3\ s^{-1}$, k_5 from $3.5 \times 10^{-11}\ cm^3\ s^{-1}$ to $5.7 \times 10^{-11}\ cm^3\ s^{-1}$, and k_7 from $4.0 \times 10^{-11}\ cm^3\ s^{-1}$ to $1.9 \times 10^{-11}\ cm^3\ s^{-1}$, approximately corresponding to 1 standard deviation changes that were enumerated in *Hudson and Reed* [1979], and the H_2O concentration was changed from 5.5 to 1.5 ppmv, certainly lower than any rocket observation at 50 km [*Hudson and Reed*, 1979]. These changes were made in the photochemical equilibrium model, and calculations were redone. This produced the species' densities given in column C of Table 2 as well as the dashed curve given in Figure 8. The level of ozone destruction at an ionization rate of $1.2 \times 10^3\ cm^{-3}\ s^{-1}$ is 6.2%, which is still lower than the 25% observed. Further unrealistic changes in k_3, k_5, k_7, and the H_2O concentration can give the ozone depletions observed, but there is no justification

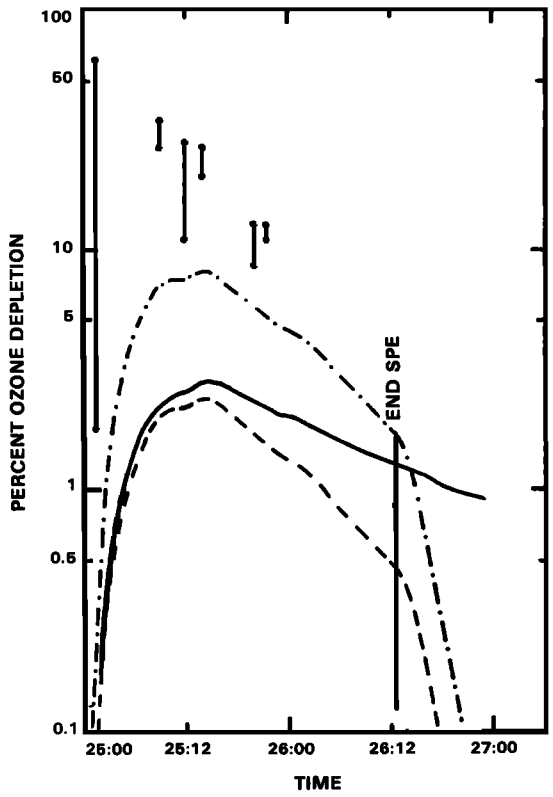

Fig. 9. A comparison of measured ozone depletion during the January 1971 SPE with theoretical results at 1 mbar (50 km). The observed and lower limit ozone depletions derived from the BUV observations are represented by the solid circles connected by straight lines. The solid curve represents a time-dependent model calculation with both SPE NO_x and HO_x production, while the dashed curve represents a similar calculation with only SPE HO_x production. The dashed-dotted curve represents a time-dependent model calculation with SPE HO_x production, modified chemistry, and low H_2O concentration. Time is given in day:hour (GMT).

for these adjustments. In fact *Turco et al.* [1981] suggest that on the basis of recent chemical kinetic data the reaction rate k_7 may be larger than 4.0×10^{-11} cm^3 s^{-1}, at least at high pressures.

7. Time-Dependent Model Results

Although the photochemical equilibrium model does provide some insight into the controlling factors of the $HO_x - O_x$ chemistry, it is an unrealistic model of the atmosphere. The atmosphere is certainly not steady state during an SPE. The SPE ionization rate changes with time (see Figure 7); consequently, the S_{HO_x} changes with time. Even with a constant S_{HO_x} rate, the atmosphere requires several hours to come to equilibrium. There are many reactions that have been neglected; among them are several inter-family reactions such as

$$HO_2 + NO \rightarrow NO_2 + OH$$

as well as others that are listed in *Johnston and Podolske* [1978].

To cope with these problems, we used the one-dimensional time-dependent model described in *Herman* [1979] adjusted to a latitude of 60°. Temperature and N_2 and O_2 profiles were taken from Cira (1972) for 60°N August at altitudes from 40 to 100 km. Since the SPE HO_x perturbation is an upper stratospheric phenomenon in the January 1971 SPE, we did not go lower than 40 km with the model. All other species, solar fluxes, reaction rates, and photoabsorption cross sections were the same as those given in *Herman* [1979] with two exceptions: first, the reaction rates and photoabsorption cross sections were updated to those of *Hudson and Reed* [1979], and, second, the chlorine species were omitted for the reasons pointed out in the discussion of the photochemical equilibrium model. Although the chlorine species become quite important in the ozone chemistry below 50 km, we are mainly concerned with the altitude regime at 50 km and above, where their effect is negligible. During normal conditions the ozone profiles resulting from the use of this model are within 20% of the observed Nimbus 4 profiles for the altitude range 40–55 km. At 50 km the calculated O_3 mixing ratio is 5.0 μgm/gm (7.6×10^{10} cm^{-3}) compared with the 4.3 μgm/gm (6.6×10^{10} cm^{-3}) observed. Other species and their densities are given in column D of Table 2.

In Figure 9 we show the percentage ozone decrease at 1 mbar (~50 km) as a function of time during the SPE of January 1971. The solid circles give the decrease we calculate from the BUV measurements. The smaller experimental value at each time of observation results from the use of the dashed line in Figure 3, while the larger experimental value results from the use of the solid line. The vertical solid lines connecting the two circles give an indication of the range of uncertainty in the observational points.

For comparison we calculate the change in ozone that current chemistry would predict from proton produced HO_x. We use the ion production profiles given in Figure 7 for the January 1971 SPE to calculate the HO_x production profiles. $S_{HO_x} = 2I_p$ is used at all altitudes. This is a good approximation at altitudes below 75 km; at altitudes above 75 km this assumption results in an upper limit HO_x specie production.

We assume a constant solar zenith angle of 75°, which is close to that observed by the Nimbus 4 satellite. The dashed line in Figure 9 is the result of this calculation at 50 km. Note that on January 25, 1971 at 1200 GMT the theortical results are about an order of magnitude smaller than the experimental results, 2.4% versus about 25%. (A similar calculation with the November 1969 SPE, in which *Weeks et al.* [1972] observed a 40% depletion at 52 km, resulted in a maximum ozone decrease of 2.7% at 50 m.) The percentage O_3 and HO_x species change are given in Figure 10 by the solid curves. This is the change occurring when the SPE is at its maximum intensity. In both O_3 and HO_x, the maximum change occurs at about the 70–73 km level.

Could the additional ozone decrease have been caused by the NO_x produced by the January 1971 SPE? We included this proton NO_x production in our calculations. The NO_x production rate in the stratosphere and mesosphere has been set equal to a variety of values ranging from 0.33 up to 2.5 NO_x species per ion pair [*Warneck*, 1972; *Brasseur and Nicolet*, 1973; *Crutzen et al.*, 1975; *Porter et al.*, 1976; *Frederick*, 1976; *Heaps*, 1978; *Fabian et al.*, 1979; *Solomon and Crutzen*, 1981; *Rusch et al.*, 1981]. This production rate varies with the altitude and with the intensity and duration of SPE [*Rusch et al.*, 1981]; however, for an event the size of the January 1971 SPE the NO_x production rate is relatively constant with altitude and time in the stratosphere and mesosphere. We set the production rate equal to 1.25 NO

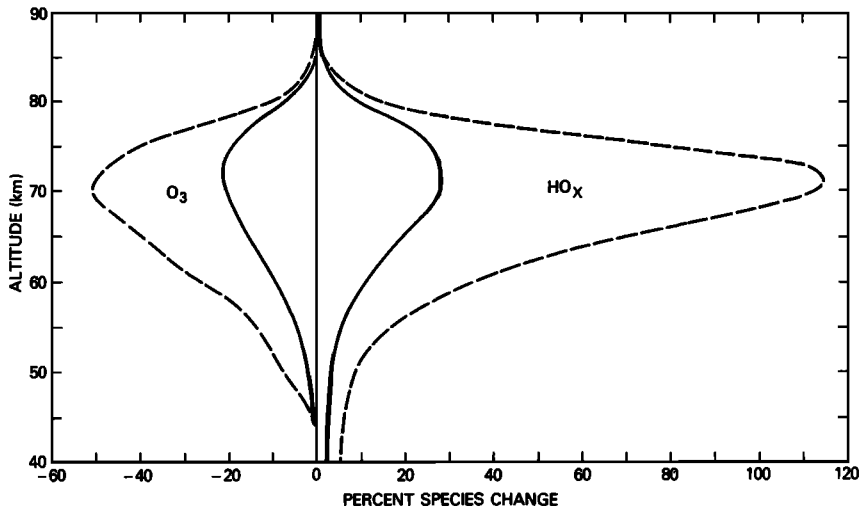

Fig. 10. Percentage ozone and HO_x species change at the maximum intensity of the January 1971 SPE. Ozone is shown as a decrease and HO_x as an increase. The solid curves present the results, using regular chemistry and reasonable H_2O concentration, in the time-dependent model. The dashed curves present the results, using modified chemistry and low H_2O concentration, in the time-dependent model.

molecules per ion pair in this calculation [*Jackman et al.*, 1979]. The time dependent model with both NO_x and HO_x produced by the SPE gave the solid curve in Figure 9. The added effect of the NO_x production is quite small although its ozone destruction persists longer than that due to HO_x. This is expected because of the longer lifetime of the NO_x species in comparison with the HO_x species.

Following our work with the photochemical equilibrium model, we also made an upper limit calculation. The reaction rates k_3, k_5, and k_7, and the H_2O concentration were all modified in the same manner as described earlier for the photochemical equilibrium mode. The ambient species densities resulting are all given in column E of Table 2. We computed the resulting O_3 decrease from the January 1971 SPE and represent these results with the dash-dot curve in Figure 9. The maximum O_3 and HO_x changes are again at the maximum intensity of the SPE and are given by the dashed lines in Figure 10. Again, the maximum O_3 decrease occurs around the 70-km level. At 50 km this modified chemistry model came closer to reproducing the undisturbed ozone concentration (see Figure 10), but the depletion predicted is still a factor of about 3 less than the observational values, 8.2% versus about 25%. Thus, even with the HO_x specie production and O_3 influence taken to this unrealistic extreme, the observed ozone destruction cannot be duplicated.

8. Conclusions

We have deduced ozone profiles during the solar proton events of January and September 1971 and August 1972 after correcting the BUV measured radiances for the direct effects of the protons on the instrument. Following the August 1972 SPEs we observe a long-term ozone depletion, lasting at least a month, in both northern and southern polar regions. This is explained as catalytic destruction of ozone by NO_x produced during the SPE. The long-term ozone depletion following the August 1972 SPEs is very clear and cannot be questioned on particle contamination grounds. Short-term ozone decreases, which we attribute to HO_x, are observed during the January 1971 SPE, even when a conservative upper limit proton correction is made. The HO_x-produced ozone depletion appears to be real and agrees with the *Weeks et al.* [1972] observation, but its magnitude is somewhat questionable because of instrument contamination. The ozone decreases in the 1971 SPEs could only be due to species with fairly short lifetimes, such as the HO_x species produced during the SPEs. But use of present chemistry and HO_x production rates do not result in the ozone decreases of the magnitude observed in the upper stratosphere. In fact, at 50 km the ozone decrease calculated by theory is an order of magnitude lower than that observed during the January 1971 SPE. An observation of an SPE by the SBUV instrument on the recently launched Nimbus-7 satellite will, it is hoped, confirm our results, since SBUV is insensitive to particles.

Appendix. Photochemical Equilibrium Model

Table 1 contains all the reactions used in this photochemical model. At 50 km altitude the main contributions to the production and loss of O_x ($O(^3P)$, $O(^1D)$, and O_3) can be written as [see, for example, *Johnston and Podolske*, 1978; *Anderson et al.*, 1980]

$$\frac{d[O_x]}{dt} = P(O_x) - L(O_x) \tag{A1}$$

where the production

$$P(O_x) = 2J_1[O_2] \tag{A2}$$

and the loss

$$L(O_x) = 2k_2[O][O_3] + 2k_3[OH][O] + 2k_8[NO_2][O] + 2k_{14}[ClO][O] \tag{A3}$$

Unless otherwise noted [O] refers to $O(^3P)$. In photochemical equilibrium $P(O_x) = L(O_x)$ so that

$$[O] = \frac{J_1[O_2]}{k_2[O_3] + k_3[OH] + k_8[NO_2] + k_{14}[ClO]} \tag{A4}$$

The production and loss of ozone can be written in a similar

manner such that

$$P(O_3) = k_1[O][O_2][M] \quad \text{(A5)}$$

and

$$L(O_3) = (J_2 + J_3)[O_3] \quad \text{(A6)}$$

Assuming photochemical equilibrium and by using (A4), (A5), and (A6) gives us a quadratic equation for (O_3) that is easily solved.

$$[O_3]^2 k_2(J_2 + J_3) + [O_3]\{(J_2 + J_3)(k_3[OH] + k_8[NO_2] + k_{14}[ClO])\} - J_1 k_1[O_2]^2[M] = 0 \quad \text{(A7)}$$

Other constituents are related to each other following a similar procedure.

$$[HO_2] = R[OH] \quad \text{(A8)}$$

with

$$R = \frac{\{k_3[O] + k_4[O_3]\}}{\{k_5[O] + k_6[O_3] + J_6\}} \quad \text{(A9)}$$

$$[O(^1D)] = \frac{J_3[O_3]}{k_{11}[N_2] + k_{12}[O_2]} \quad \text{(A10)}$$

$$[NO_2] = \frac{k_9[O_3][NO]}{k_8[O] + J_5} \quad \text{(A11)}$$

$$[ClO] = \frac{k_{13}[Cl][O_3]}{k_{14}[O]} \quad \text{(A12)}$$

$$[Cl] = \frac{k_{15}[OH][HCl]}{k_{16}[HO_2] + k_{18}[CH_4]} \quad \text{(A13)}$$

We assume that the SPE will add S_{HO_x} to the HO_x production. The production and loss of the HO_x species are thus written

$$P(HO_x) = 2k_{10}[H_2O][O(^1D)] + 2J_4[H_2O] + J_7[HCl] + J_8[HOCl] + S_{HO_x} \quad \text{(A14)}$$

$$L(HO_x) = 2k_7[OH][HO_2] + k_{15}[OH][HCl] + k_{16}[Cl][HO_2] + k_{17}[HO_2][ClO] \quad \text{(A15)}$$

An easily solved quadratic equation is found for [OH] when (A8), (A14), and (A15) are used.

$$[OH]^2 2k_7 R + [OH]\{k_{15}[HCl] + k_{16}R[Cl] + k_{17}R[ClO]\} - 2k_{10}[H_2O][O(^1D)] - 2J_4[H_2O] - J_7[HCl] \cdot J_8[HOCl] - S_{HO_x} = 0 \quad \text{(A16)}$$

Acknowledgments. The authors would like to acknowledge the useful discussions with R. S. Stolarski, J. R. Herman, J. E. Frederick, and D. F. Heath (all at the Goddard Space Flight Center), Susan Solomon (National Center for Atmospheric Research), and would also like to thank C. J. McQuillan (Goddard Space Flight Center) for providing helpful insight into the computer programming aspects of this work. CHJ wishes to thank the National Academy of Sciences for a resident research associateship at the Goddard Space Flight Center during which most of this work was carried out.

References

Anderson, J. G., H. J. Grassl, R. E. Shetter, and J. J. Margitan, Stratospheric free chlorine measured by balloon-borne in situ resonance fluorescence, *J. Geophys. Res., 85,* 2869–2887, 1980.

Borucki, W. J., D. S. Colburn, R. C. Whitten, L. A. Capone, and M. Covert, Model analysis of the ozone depletion due to the August 1972 solar proton event, *Eos Trans. AGU, 59,* 284, 1978.

Brasseur, G., and M. Nicolet, Chemospheric processes of nitric oxide in the mesosphere and stratosphere, *Planet. Space Sci., 21,* 939–961, 1973.

Crutzen, P. J., and S. Solomon, Response of mesospheric ozone to particle precipitation, *Planet. Space Sci., 28,* 1147–1153, 1980.

Crutzen, P. J., I. S. A. Isaksen, and G. C. Reid, Solar proton events: Stratospheric sources of nitric oxide, *Science, 189,* 457–458, 1975.

DeMore, W. B., L. J. Stief, F. Kaufman, D. M. Golden, R. F. Hampson, M. J. Kurylo, J. J. Margitan, M. J. Molina, and R. T. Watson, Chemical kinetic and photochemical data for use in stratospheric modelling, *Publ. 81-3,* Jet Propul. Lab., Calif. Inst. of Tech., Pasadena, Calif., 1981.

Fabian, P., J. A. Pyle, and R. J. Wells, The August 1972 solar proton event and the atmospheric ozone layer, *Nature, 277,* 458–460, 1979.

Frederick, J. E., Solar corpuscular emission and neutral chemistry in the earth's middle atmosphere, *J. Geophys. Res., 81,* 3179–3186, 1976.

Heaps, M. G., The effect of a solar proton event on the minor neutral constituents of the summer polar mesosphere, *Rep. ASL-TR-0012,* U.S. Army Atmos. Sci. Lab., White Sands, N. M., 1978.

Heath, D. F., A. J. Krueger, and P. J. Crutzen, Solar proton event: Influence on stratospheric ozone, *Science, 197,* 886–889, 1977.

Herman, J. R., The response of stratospheric constituents to a solar eclipse, sunrise, and sunset, *J. Geophys. Res., 84,* 3701–3710, 1979.

Hudson, R. D., and E. I. Reed (Eds.), The stratosphere: Present and future, *NASA Ref. Pub. 1049,* 1979.

Jackman, C. H., H. S. Porter, and J. E. Frederick, Upper limits on production rate of NO per ion pair, *Nature, 280,* 170, 1979.

Jackman, C. H., J. E. Frederick, and R. S. Stolarski, Production of odd nitrogen in the stratosphere and mesosphere: An intercomparison of source strengths, *J. Geophys. Res., 85,* 7495–7505, 1980.

Johnston, H. S., and J. Podolski, Interpretations of stratospheric photochemistry, *Rev. Geophys. Space Phys., 16,* 491–519, 1978.

McPeters, R. D., The behavior of ozone near the stratopause from two years of BUV observations, *J. Geophys. Res., 85,* 4545–4550, 1980.

National Oceanic and Atmospheric Administration, *Solar-Geophysical Data,* no. 328, pp. 68–73, 1971.

Porter, H. S., C. H. Jackman, and A. E. S. Green, Efficiencies for production of atomic nitrogen and oxygen by relativistic proton impact in air, *J. Chem. Phys., 65,* 154–167, 1976.

Reagan, J. B., R. E. Meyerott, R. W. Nightingale, R. C. Gunton, R. G. Johnson, J. E. Evans, W. L. Imhof, D. F. Heath, and A. J. Krueger, Effects of the August 1972 solar particle events on stratospheric ozone, *J. Geophys. Res., 86,* 1473–1494, 1981.

Reid, G. C., I. S. A. Isaksen, T. E. Holzer, and P. J. Crutzen, Influence of ancient solar-proton events on the evolution of life, *Nature, 259,* 177–179, 1976.

Rusch, D. W., J. C. Gerard, S. Solomon, P. J. Crutzen, and G. C. Reid, The effect of particle precipitation events on the neutral and ion chemistry of the middle atmosphere, I, Odd nitrogen, *Planet. Space Sci., 29,* 767–774, 1981.

Solomon, S., and P. J. Crutzen, Analysis of the August 1972 solar proton event including chlorine chemistry, *J. Geophys. Res., 86,* 1140–1146, 1981.

Solomon, S., D. W. Rusch, J.-C. Gerard, G. C. Reid, and P. J. Crutzen, The effect of particle precipitation events on the neutral and ion chemistry of the middle atmosphere, II, Odd hydrogen, *Planet. Space Sci., 29,* 885–894, 1981.

Swider, W., and T. J. Keneshea, Decrease of ozone and atomic oxygen in the lower mesosphere during a PCA event, *Planet. Space Sci., 21,* 1969–1973, 1973.

Swider, W., T. J. Keneshea, and C. I. Foley, An SPE-disturbed *D*-region model, *Planet. Space Sci., 26,* 883–892, 1978.

Turco, R. P., R. C. Whitten, O. B. Toon, E. C. Y. Inn, and P. Hamill, Stratospheric hydroxyl radical concentrations: New limitations suggested by observations of gaseous and particulate sulfur, *J. Geophys. Res., 86,* 1129–1139, 1981.

Warneck, P., Cosmic radiation as a source of odd nitrogen in the stratosphere, *J. Geophys. Res., 77,* 6589–6591, 1972.

Weeks, L. H., R. S. CuiKay, and J. R. Corbin, Ozone measurements in the mesosphere during the solar proton event of November 2, 1969, *J. Atmos. Sci., 29,* 1138–1142, 1972.

(Received December 3, 1980;
revised May 6, 1981;
accepted September 1, 1981.)